Stem Cell Reports
Report
ISSCR
OPEN ACCESS

In Vivo Therapeutic Potential of Mesenchymal Stromal Cells Depends on the Source and the Isolation Procedure

Francesca Bortolotti,[1,4] Laura Ukovich,[1,4] Vahid Razban,[1,2] Valentina Martinelli,[1] Giulia Ruozi,[1] Barbara Pelos,[3] Franca Dore,[3] Mauro Giacca,[1] and Serena Zacchigna[1,*]
[1]Molecular Medicine Laboratory, International Centre for Genetic Engineering and Biotechnology (ICGEB), 34149 Trieste, Italy
[2]Tissue Engineering Department, Shiraz University of Medical Sciences, School of Advanced Medical Sciences and Technologies, Shiraz 7134814336, Iran
[3]Struttura Complessa di Medicina Nucleare, "Ospedali Riuniti," 34142 Trieste, Italy
[4]Co-first author
*Correspondence: zacchign@icgeb.org
http://dx.doi.org/10.1016/j.stemcr.2015.01.001

SUMMARY

Over the last several years, mesenchymal stromal cells (MSCs) have been isolated from different tissues following a variety of different procedures. Here, we comparatively assess the ex vivo and in vivo properties of MSCs isolated from either adipose tissue or bone marrow by different purification protocols. After MSC transplantation into a mouse model of hindlimb ischemia, clinical and histological analysis revealed that bone marrow MSCs purified on adhesive substrates exerted the best therapeutic activity, preserving tissue viability and promoting formation of new arterioles without directly transdifferentiating into vascular cells. In keeping with these observations, these cells abundantly expressed cytokines involved in vessel maturation and cell retention. These findings indicate that the choice of MSC source and purification protocol is critical in determining the therapeutic potential of these cells and warrant the standardization of an optimal MSC isolation procedure in order to select the best conditions to move forward to more effective clinical experimentation.

INTRODUCTION

Mesenchymal stromal cells (MSCs) are defined as multipotent, self-renewing cells residing in several tissues, including the bone marrow, adipose tissue, umbilical cord blood, and placenta (Pittenger et al., 1999). These cells are defined as multipotent, as they are capable of generating different mesenchymal cell types, traditionally adipocytes, chondrocytes, and osteocytes, but also smooth muscle cells and cardiomyocytes (Makino et al., 1999; Pittenger et al., 1999). MSCs have been at the forefront of clinical research for the therapy of cardiovascular disorders for many years. In particular, cardiac and peripheral ischemia is a leading cause of morbidity and mortality in our aging society and suffers from a lack of curative therapies (Tendera et al., 2011). In this setting, MSC transplantation has been proposed as an innovative therapy for no-option ischemic patients. Originally, the therapeutic potential of these cells was thought to arise through their putative capacity to transdifferentiate, thereby directly contributing to vasculogenesis and tissue regeneration (Quevedo et al., 2009). This attractive hypothesis led to the prompt, perhaps immature transition of the results obtained in animal models to the clinics, with the ambitious goal to regenerate ischemic tissues (Hare et al., 2009; Tateishi-Yuyama et al., 2002). However, MSC plasticity has been later harshly questioned (Noiseux et al., 2006), and the therapeutic potential of these cells is currently considered to derive from the secretion of a variety of growth factors and cytokines exerting a paracrine, protective effect on ischemic cells (Gnecchi et al., 2012).

Despite the common definition of MSCs and the modest but real therapeutic effect exerted by these cells in various experimental and clinical settings, there is no universal agreement on the optimal source and method for MSC isolation and culture (Soleimani and Nadri, 2009; Sung et al., 2008; Yamamoto et al., 2007). This importantly limits the possible comparison of the observed results in terms of MSC characterization and therapeutic activity. Most of the studies that compared different MSC types are based on the analysis of surface markers, multipotency, and angiogenic assays ex vivo (Lee et al., 2004; Peng et al., 2008). A few studies also compared MSC activity in vivo, in animal models of cardiac and limb ischemia, but they considered either different tissue sources (van der Bogt et al., 2009) or different purification methods (Seeger et al., 2007) and never the combination of the two parameters. Additional relevant variables in these studies are the species from which MSCs were isolated and the specific animal model used to ascertain their therapeutic properties. This again prevents the direct comparison of most of the existing studies and warrants the prospective characterization of MSCs derived from various tissues and purified according to different purification protocols.

Here, we provide evidence that murine MSCs, harvested from either adipose tissue or bone marrow and following

different purification procedures, behave differently and, most importantly, exhibit different therapeutic potential in a mouse model of critical limb ischemia (CLI). This underlines the need to adopt optimal and standardized methods for MSC processing in future preclinical and clinical trials.

RESULTS

MSCs Isolated from Different Sources and according to Different Procedures Show a Common Phenotype

To identify the optimal population of MSCs to treat hindlimb ischemia, cells were purified from either the adipose tissue or the bone marrow of mice using three different protocols. Adipose tissue (AT) MSCs were isolated by tissue digestion followed by centrifugation, while bone marrow (BM)-derived MSCs were obtained by either frequent medium changes (BM-MSCs) or immunodepletion (iBM-MSCs) (Figure 1A). In all three cases, the first MSC colonies appeared after a few days and cells were cultured until they reached 80% confluence (within ~10 days for AT-MSCs and ~6 weeks for both types of BM-derived cells). When assessing their proliferative potential, iBM-MSCs appeared to grow significantly faster than the other populations (Figure 1B). When seeded at a low number, all three MSC cell types formed a similar number of colonies, confirming their clonogenic potential (Figures 1C and 1D). Despite their high proliferative capacity, MSCs did not become immortal but started to express the senescence-associated β-galactosidase (SA-βgal) marker at passage 12 (Figure S1A available online) and stopped multiplying after an additional three to six passages.

Regardless of their different origin and isolation protocol, the three cell populations exhibited a very similar marker profile. They abundantly expressed the MSC-defining CD44, CD105, CD29, and CD90 markers, whereas they scored negative for endothelial (CD31), myeloid (CD11b, GR-1), or hematopoietic (CD45 and CD34) antigens (Boxall and Jones, 2012). Low levels of expression were also found for SCA-1, c-KIT, TIE-2, CXCR4, and TER-119 (Figures 1E and S1B; Table S1).

Finally, AT-MSCs, iBM-MSCs, and BM-MSCs were probed for their capacity to differentiate into adipocytes, chondrocytes, and osteocytes. Adipogenic medium induced the appearance of lipid vacuoles, positive to oil red staining; chondrogenic medium forced the cells to accumulate alcian blue-positive proteoglycans; and osteogenic medium dramatically induced accumulation of intracellular calcium deposits, reactive to Alizarin staining (Figure 1F). These results confirm the multipotency of the three MSC populations.

Transplantation of AT-MSCs, iBM-MSCs, and BM-MSCs Markedly Reduces Severe Hindlimb Ischemia

We assessed MSC therapeutic potential in a mouse model of hindlimb ischemia induced by removal of the entire femoral artery. The day following surgery, the animals received 2×10^5 cells (or medium as control) in the limb homolateral to ischemia (Figure 2A). Clinical follow-up over 3 weeks showed a significant improvement in the group injected with iBM-MSCs, but the most significant improvement was seen in the group injected with BM-MSCs (Figure 2B). Histological analysis of muscle sections at day 21 showed extensive necrosis, adipose substitution, and marked infiltration by inflammatory cells in control animals. In contrast, the muscles injected with any MSC population showed a statistically significant reduction of the inflammatory infiltrate (Figures 2C and 2D), associated with a smaller lesion area (Figures 2C and 2E). In addition, the number of regenerating fibers, characterized by central nuclei, was significantly higher in animals treated with cells of BM origin, in particular in the case of BM-MSCs (Figures 2C and 2F). Thus, postischemic administration of any MSC type, but mostly of BM-MSCs, remarkably improves functional and structural recovery of the ischemic limb.

MSCs Induce Neovascularization in Ischemic Muscles

To assess the angiogenic potential of MSCs, muscles were double labeled with lectin, which stains endothelial and mononuclear cells, and antibodies against α-smooth muscle actin (α-SMA), which marks smooth muscle cells (SMCs) surrounding arterial vessels (Figure 3A). Whereas no significant difference in the number of lectin-positive cells was detected, all three MSC populations stimulated a massive formation of 10–100 μm arterioles (Figure 3B). This effect was particularly pronounced in the case of BM-MSCs.

Lead by recent literature supporting the paracrine activity of MSCs (Gnecchi et al., 2012; Mirotsou et al., 2011), we analyzed the mRNA levels of a series of molecules involved in blood vessel formation and maturation (Figure 3C). BM-MSCs were found to express particularly abundant levels of factors required for vessel stabilization, SMC migration, and matrix remodeling, such as *Tgf-β*, *Pdgf-β*, and *Mmp9*. In addition, these cells also expressed high levels of *Ccl5* and *Sdf-1α*, two chemokines known to be involved in the recruitment and retention of proangiogenic macrophages and MSCs themselves (Abbott et al., 2004; Chen et al., 2008). Thus MSCs, and in particular BM-MSCs, express a cocktail of soluble factors able to enhance their retention in an autocrine manner and also attract proangiogenic cells. To confirm the latter concept experimentally, we performed a

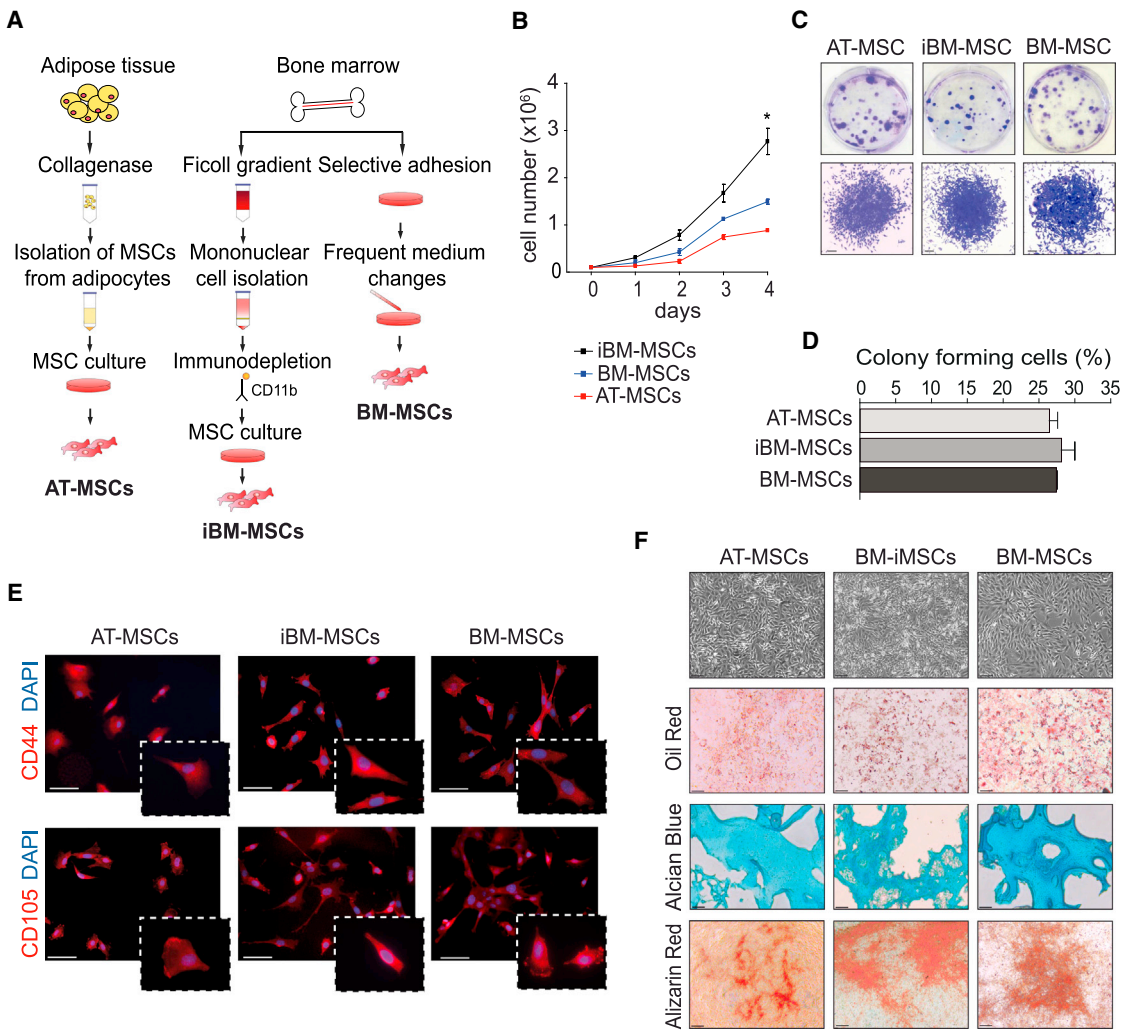

Figure 1. Characterization of MSCs Isolated according to Three Different Procedures

(A) Schematic overview of MSCs isolation procedures.

(B) Counting of AT-MSCs, BM-MSCs, and iBM-MSCs for 4 consecutive days. Data (n = 3 biological replicates) are presented as mean ± SEM (*p < 0.05).

(C) Crystal violet staining of MSCs showing colonies after 10 days of culture (upper panels) and a representative colony (lower panels). Scale bar, 100 μm.

(D) Quantification of colonies formed after 10 days of cell culture. Data (n = 3 biological replicates) are presented as mean ± SEM.

(E) MSC immunophenotyping at passage 3. CD44 or CD105, red; DAPI, blue; scale bar, 50 μm.

(F) All MSCs exhibited a similar morphology and became positive for oil red (adipocytic differentiation; scale bar, 50 μm), alcian blue (chondrocytic differentiation; scale bar 50 μm), and alizarin red (osteocytic differentiation; scale bar, 80 μm).

migration assay and found that BM-MSCs were the only cell type able to attract murine SMCs (Figures 3D and 3E), similar to 10% fetal bovine serum (used as positive control) and consistent with their abundant expression of *Pdgf-β* at the mRNA and protein level (Figures 3C and S2) (Gerthoffer, 2007). The ample production of proangiogenic cytokines by the various MSCs suggested that the same promigratory effect could be achieved by the delivery of their conditioned medium (CM). To explore this possibility, we injected the medium harvested from the same number of AT-MSCs, iBM-MSCs, and BM-MSCs (2×10^5) used in the previous experiment, at days 1, 3, and 7 after surgery. This treatment resulted in a clear trend toward improvement in all the morphological and functional parameters analyzed (Figure S3).

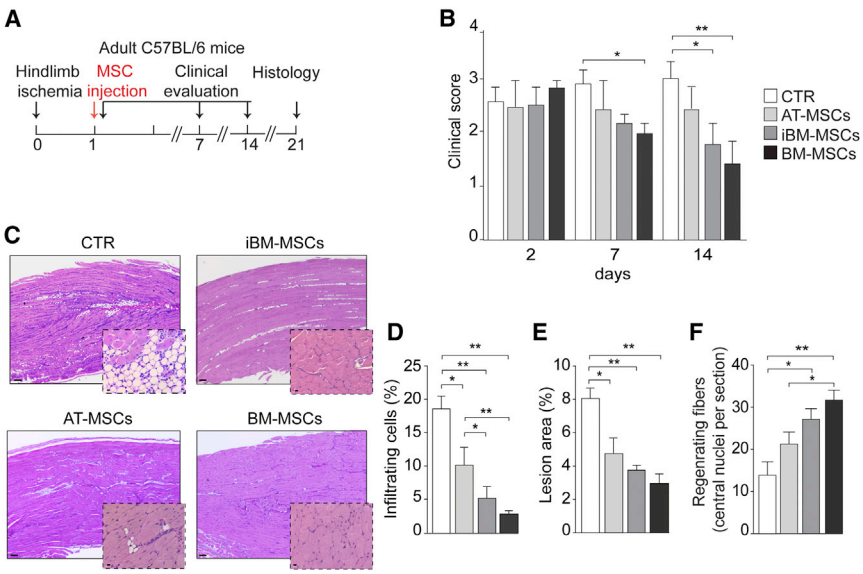

Figure 2. Morphological and Functional Evaluation of the Therapeutic Effect of MSCs

(A) CLI experimental flow chart. Mice were injected with AT-MSCs, BM-MSCs, or iBM-MSCs at passage 3–5 or medium (n = 10 animals per group).

(B) Limb function evaluation at days 2, 7, and 21 after CLI according to the criteria described in Table S2.

(C) Representative hematoxylin-eosin staining of ischemic muscle from untreated and treated animals at day 21. Scale bar represents 100 μm for lower magnification and 10 μm for higher magnification.

(D) Percentage of infiltrating cells at the site of ischemia.

(E) Percentage of muscle affected by ischemic damage.

(F) Quantification of central nuclei as a hallmark of muscle regeneration.

Data in (B) and (D)–(F) are expressed as mean ± SEM (n = 10 animals per group; *p < 0.05, **p < 0.01).

BM-MSCs Stimulate Functional Neovascularization but Are Not Incorporated in the Newly Formed Vasculature

Functional muscle perfusion was evaluated by planar scintigraphy (Figures 4 and S4). In control animals, a large perfusion deficit was evident at day 1 and was still present 2 weeks after ischemia. A statistically significant improvement that was evident starting at day 7 after injection was detected in the animals treated with BM-MSCs (Figures 4B and 4C). A moderate recovery was detected in iBM-MSC-treated animals at 1 week, while AT-MSCs did not provide any benefit compared to controls. Thus, BM-MSCs were the most effective cells in inducing functional vascularization.

We then explored the possible mechanisms responsible for the superior performance of BM-MSCs. We observed that BM-MSCs and AT-MSCs resisted doxorubicin- or hydrogen-peroxide-induced apoptosis more than iBM-MSCs, as evaluated by caspase-3/7 activation and Annexin V staining (Figures 4D and 4E). When analyzing their persistence into ischemic muscles in vivo, we found that the engraftment of BM-MSCs was significantly higher at day 21 compared to the other two MSC types (Figures 4F and 4G). To investigate whether these cells directly contributed to the formation of new vessels by transdifferentiation, we evaluated the colocalization of 1,1′-dioctadecyl-3,3,3′,3′-tetramethylindocarbocyanine perchlorate (DiI)-labeled MSCs with endothelial (CD31) and SMC (α-SMA) markers. The complete lack of colocalization (Figures 4H and 4I) further supports a paracrine mechanism responsible for their angiogenic properties.

DISCUSSION

This study provides a comparison of the therapeutic properties of three MSC populations isolated from two different tissues (BM and AT) according to different purification protocols. Our results show that (1) the three MSC types acquire similar phenotypic and functional properties after the first passages, (2) any MSC type provides therapeutic benefit after CLI, (3) BM-MSCs perform better than the other types in preserving tissue viability and inducing neovascularization, and (4) BM-MSCs do not transdifferentiate in vivo into vascular structures but persist longer and act in a paracrine manner to promote vascular formation.

The first objective of this study was the definition of an optimal protocol for MSC isolation. We intentionally focused on BM and AT, as these are the most accessible tissues for MSC recovery. Current protocols for AT-MSC isolation are almost universally based on tissue digestion; for the BM, instead, we selected the two most frequently used methods, namely isolation based on MSC adhesive properties (BM-MSCs) (Soleimani and Nadri, 2009) and density gradient centrifugation, followed by immunodepletion (iBM-MSCs) (Sung et al., 2008).

Despite presenting a similar behavior in cell culture, the three MSC types showed a different therapeutic potential once injected in vivo in a CLI model, reducing necrosis and inflammation and stimulating muscle regeneration, although at a different extent. They also prompted the formation of functional arterioles, in accordance with previous reports (Cho et al., 2009; Iwase et al., 2005).

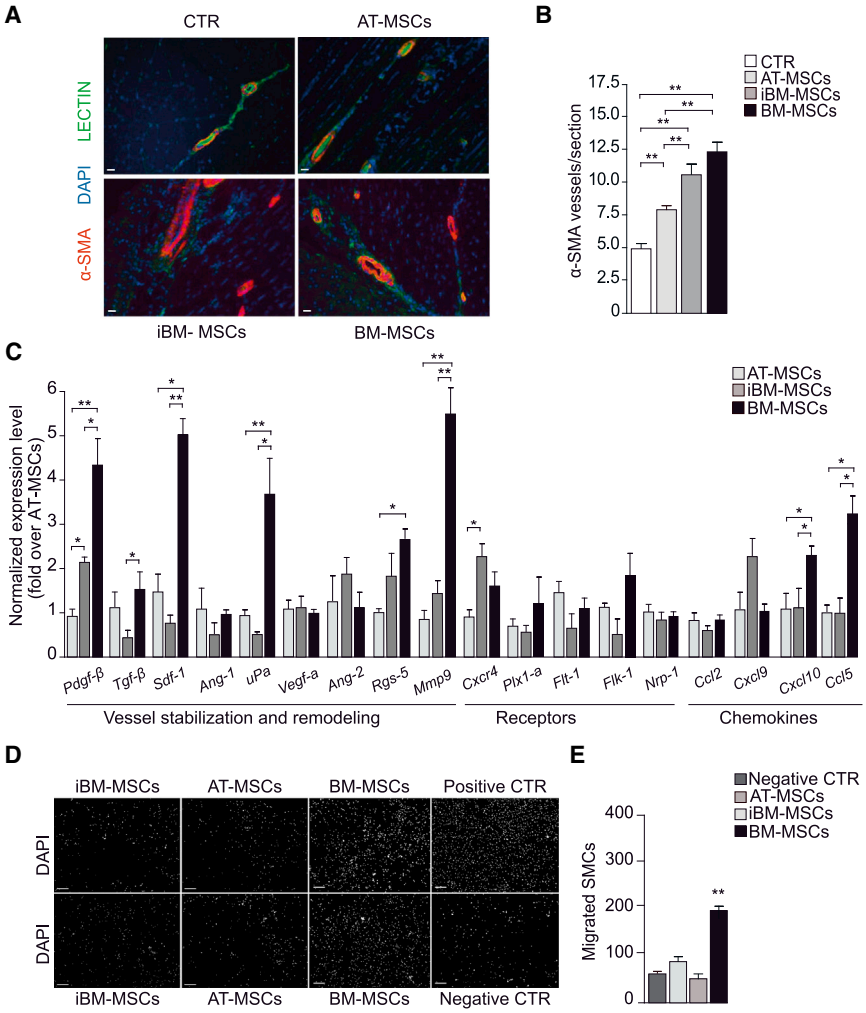

Figure 3. MSC Treatment Effectively Induces Neovascularization in Ischemic Muscles

(A) Representative immunostaining for vascular structures at day 21. α-SMA, red; lectin, green; DAPI, blue; scale bar, 50 μm.

(B) Number of α-SMA positive vessels. Data (n = 10 animals per group) are expressed as mean ± SEM (*p < 0.05, **p < 0.01).

(C) Quantification of mRNA levels of factors involved in angiogenesis, vessel stabilization, and remodeling (n = 3 biological replicates). Expression of each gene was first normalized over *Gapdh* and then over AT-MSCs.

(D) Representative images of murine SMCs migrated in response to the various MSCs. SMCs were seeded on the upper chamber and stained with DAPI after migration to the bottom side of the filter. MSCs were seeded in the lower chamber (n = 3 biological replicates). Serum-free medium and serum-rich medium were used as negative and positive controls; scale bar, 100 μm.

(E) Quantification of SMCs migrated in response to the various MSCs, expressed as number of migrated cells per 100× field. Data in (B), (C), and (E) are expressed as mean ± SEM (*p < 0.05, **p < 0.01).

Interestingly, this was better accomplished by BM-MSCs, which abundantly secreted soluble cytokines involved in vessel remodeling and stabilization (such as PDGF-β) and induced the migration of vascular SMCs. This contradicts the findings of Kim et al., who attributed a higher angiogenic and therapeutic potential to AT-MSCs in comparison to MSCs of BM origin (Kim et al., 2007). A few differences can explain this discrepancy. First, their BM-MSCs were purified by density gradient centrifugation, while our results clearly indicate that the therapeutic potential strictly depends on the isolation protocol. Second, they transplanted human cells into nude mice, which did not allow for the assessment of the immunemodulatory action of MSCs.

Although multiple evidence points toward vascular endothelial growth factor (*Vegf*) as the main angiogenic cytokine secreted by MSCs (Kinnaird et al., 2004), we did not observe significant differences in *Vegf* expression among the three MSC types. Instead, the major differences occurred in genes involved in SMC recruitment and matrix remodeling (*Tgf-β*, *Pdgf-β*, and *Mmp9*), which are two essential events for the proper maturation of arterial vessels (Zacchigna et al., 2008). Can this arteriogenic effect be recapitulated by the delivery of the MSC supernatant? Although not reaching statistical significance, probably due to the relatively low number of animals analyzed, the repeated injection of CM from the three MSC types resulted in a trend toward improvement, fully consistent with the results observed upon cell transplantation. This supports the conclusion that the MSC secretome could recapitulate the effect of MSC injection (Ranganath et al., 2012), but its effectiveness is most likely dampened by the short half-life of its molecules. These results leave at least two open questions. First, CM and MSC transplantation were not performed on the same set of animals, and thus we cannot exclude interanimal variability when comparing the efficacy of the two treatments. Second, we did not investigate whether the injection of higher CM amounts

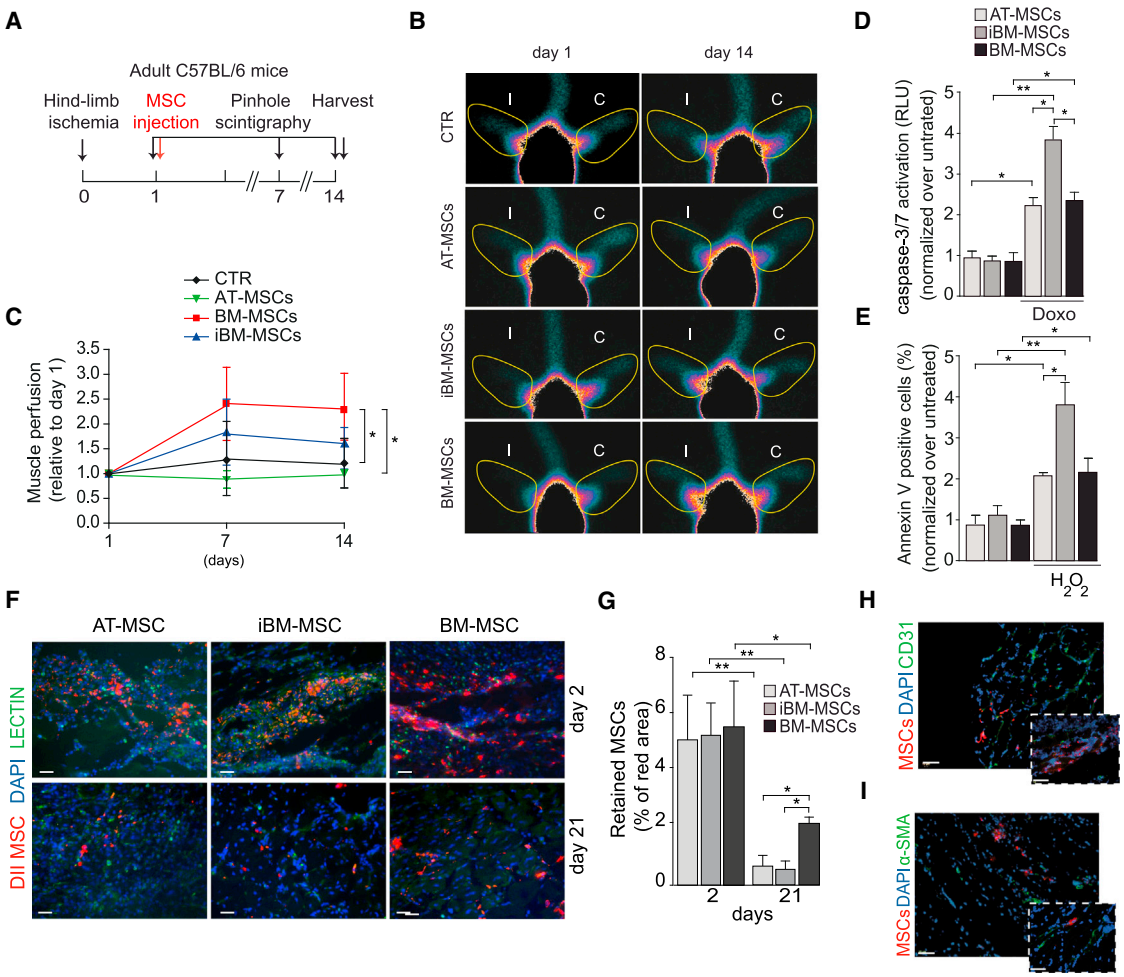

Figure 4. MSCs Induce Functional Vascularization but Do Not Differentiate into Vascular Structures In Vivo

(A) Planar scintigraphy experimental flow chart (n = 8 animals per group).

(B) Representative images showing the regions of interest (yellow line) used to quantify muscle perfusion on the ischemic (I) and control (C) limb at the indicated time points.

(C) Quantification of muscle perfusion, normalized over the perfusion measured at day 1.

(D) Level of caspase activation in MSCs exposed to doxorubicin, normalized over untreated cells (n = 9, 3 biological and 3 technical replicates).

(E) Percentage of Annexin V+ cells after exposure to H_2O_2, normalized over untreated cells (n = 9, 3 biological and 3 technical replicates).

(F) Representative images of MSC engraftment at days 2 and 21. DiI-labeled MSCs, red; lectin, green; DAPI, blue; scale bar, 50 μm.

(G) Quantification of cell engraftment at the indicated time points (n = 6 animals per group).

(H) Representative images of DiI-labeled BM-MSCs (red) stained for CD31 (green). Nuclei are counterstained with DAPI (blue). Scale bar represents 25 μm for lower magnification and 40 μm for higher magnification.

(I) Representative images of DiI-labeled BM-MSCs (red) stained for α-SMA (green). Nuclei are counterstained with DAPI (blue). Scale bars as in (H).

Data in (C)–(E) and (G) are expressed as mean ± SEM (*p < 0.05, **p < 0.01).

or the administration of more frequent doses would result in a better outcome.

An additional reason for the higher therapeutic activity of BM-MSCs could be related to the longer engraftment and survival of the cells in vivo. In any case, it appears important to remark that our MSCs did not become immortalized, as they underwent cellular senescence after passage 12 and we never observed formation of tumor masses during long-term follow-up.

In conclusion, our findings indicate that BM-MSCs are the most effective MSC type to improve perfusion and functional recovery after hindlimb ischemia. In contrast

to initial studies supporting MSC plasticity (Quevedo et al., 2009), these cells were not able to transdifferentiate into either endothelial cells or SMCs while exerting their effect through a paracrine mechanism.

EXPERIMENTAL PROCEDURES

MSC Culture and In Vivo Experiments

MSCs were isolated from the AT or BM of C57/BL6 mice according to three adapted protocols (Soleimani and Nadri, 2009; Sung et al., 2008; Yamamoto et al., 2007). Cells (2×10^5) at passage 3–5 were injected into the hindlimb of syngeneic mice the day following resection of the femoral artery. Mice were monitored clinically and by planar scintigraphy and sacrificed at day 21 for histological analysis. Animal care and treatment were conducted in conformity with institutional guidelines, in compliance with national and international laws and policies (European Economic Community Council Directive 86/609, OJL 358, December 12th, 1987, and UE2010763), after institutional review board approval.

MSC Phenotypic Characterization

MSC-specific surface antigens were analyzed by flow cytometry and immunofluorescence. Clonogenic potential was evaluated upon staining with crystal violet. Differentiation was performed using a dedicated kit from LifeLine Cell Technologies.

Histology and Immunofluorescence

Muscle sections were stained with hematoxylin-eosin to perform morphometric analysis, with fluorescein isothiocyanate (FITC)-conjugated lectin and anti-α-SMA antibodies to stain the vasculature. Cells were labeled with DiI prior injection to track cell engraftment.

Real-Time PCR

Total RNA was extracted using TRIzol and reverse transcribed using hexameric random primers. All the amplifications were performed on a Bio-Rad real-time thermal cycler CFX96 using TaqMan probes (Applied Biosystems).

Migration Assay

Murine SMC migration in response to MSC supernatant was performed using 8 μm transwell supports (Costar, Corning).

Apoptosis Assay

MSC apoptosis was induced by hydrogen peroxide (H_2O_2) or doxorubicin and quantified either by flow cytometry using the Annexin V-FITC Apoptosis Detection Kit (Roche) or by using the Caspase-Glo 3/7 Assay System (Promega).

Statistical Analysis

All in vitro experiments were repeated at least three times and performed including at least three biological replicates. Data are presented as mean and SEM. Comparison within groups was analyzed by ANOVA (followed by Bonferroni post hoc analysis) for the evaluation based on tissue sections. In the case of experiments entailing the follow-up of the same animals over multiple time points, we used repeated-measures ANOVA to analyze statistical significance of the differences between groups over time. $p < 0.05$ was considered as statistically significant.

Additional details on the experimental procedures used in this work are available in Supplemental Experimental Procedures.

SUPPLEMENTAL INFORMATION

Supplemental Information includes Supplemental Experimental Procedures, four figures, and three tables and can be found with this article online at http://dx.doi.org/10.1016/j.stemcr.2015.01.001.

AUTHOR CONTRIBUTIONS

F.B. performed purification and characterization of MSCs. L.U. performed the in vivo experiments. V.R. and V.M. contributed to MSC purification and culture. B.P. and F.D. performed scintigraphy experiments. G.R. and M.G. critically evaluated the research approach and results. S.Z. planned the experiments and wrote the manuscript.

ACKNOWLEDGMENTS

This work was supported by Advanced Grant 250124 from the European Research Council (ERC), the Fondation Leducq's Transatlantic Networks of Excellence Program, projects FIRB RBAP11Z4Z9 and PRIN 2010RNXM9C from the MIUR (Italy), and project CTC from the Fondazione CRTrieste (Italy) to M.G. The authors are grateful to Suzanne Kerbavcic for precious editorial assistance.

Received: August 6, 2014
Revised: January 2, 2015
Accepted: January 2, 2015
Published: February 5, 2015

REFERENCES

Abbott, J.D., Huang, Y., Liu, D., Hickey, R., Krause, D.S., and Giordano, F.J. (2004). Stromal cell-derived factor-1alpha plays a critical role in stem cell recruitment to the heart after myocardial infarction but is not sufficient to induce homing in the absence of injury. Circulation *110*, 3300–3305.

Boxall, S.A., and Jones, E. (2012). Markers for characterization of bone marrow multipotential stromal cells. Stem Cells Int. *2012*, 975871.

Chen, L., Tredget, E.E., Wu, P.Y., and Wu, Y. (2008). Paracrine factors of mesenchymal stem cells recruit macrophages and endothelial lineage cells and enhance wound healing. PLoS One *3*, e1886.

Cho, H.H., Kim, Y.J., Kim, J.T., Song, J.S., Shin, K.K., Bae, Y.C., and Jung, J.S. (2009). The role of chemokines in proangiogenic action induced by human adipose tissue-derived mesenchymal stem cells in the murine model of hindlimb ischemia. Cell. Physiol. Biochem. *24*, 511–518.

Gerthoffer, W.T. (2007). Mechanisms of vascular smooth muscle cell migration. Circ. Res. *100*, 607–621.

Gnecchi, M., Danieli, P., and Cervio, E. (2012). Mesenchymal stem cell therapy for heart disease. Vascul. Pharmacol. *57*, 48–55.

Hare, J.M., Traverse, J.H., Henry, T.D., Dib, N., Strumpf, R.K., Schulman, S.P., Gerstenblith, G., DeMaria, A.N., Denktas, A.E., Gammon, R.S., et al. (2009). A randomized, double-blind, placebo-controlled, dose-escalation study of intravenous adult human mesenchymal stem cells (prochymal) after acute myocardial infarction. J. Am. Coll. Cardiol. *54*, 2277–2286.

Iwase, T., Nagaya, N., Fujii, T., Itoh, T., Murakami, S., Matsumoto, T., Kangawa, K., and Kitamura, S. (2005). Comparison of angiogenic potency between mesenchymal stem cells and mononuclear cells in a rat model of hindlimb ischemia. Cardiovasc. Res. *66*, 543–551.

Kim, Y., Kim, H., Cho, H., Bae, Y., Suh, K., and Jung, J. (2007). Direct comparison of human mesenchymal stem cells derived from adipose tissues and bone marrow in mediating neovascularization in response to vascular ischemia. Cell. Physiol. Biochem. *20*, 867–876.

Kinnaird, T., Stabile, E., Burnett, M.S., Shou, M., Lee, C.W., Barr, S., Fuchs, S., and Epstein, S.E. (2004). Local delivery of marrow-derived stromal cells augments collateral perfusion through paracrine mechanisms. Circulation *109*, 1543–1549.

Lee, R.H., Kim, B., Choi, I., Kim, H., Choi, H.S., Suh, K., Bae, Y.C., and Jung, J.S. (2004). Characterization and expression analysis of mesenchymal stem cells from human bone marrow and adipose tissue. Cell. Physiol. Biochem. *14*, 311–324.

Makino, S., Fukuda, K., Miyoshi, S., Konishi, F., Kodama, H., Pan, J., Sano, M., Takahashi, T., Hori, S., Abe, H., et al. (1999). Cardiomyocytes can be generated from marrow stromal cells in vitro. J. Clin. Invest. *103*, 697–705.

Mirotsou, M., Jayawardena, T.M., Schmeckpeper, J., Gnecchi, M., and Dzau, V.J. (2011). Paracrine mechanisms of stem cell reparative and regenerative actions in the heart. J. Mol. Cell. Cardiol. *50*, 280–289.

Noiseux, N., Gnecchi, M., Lopez-Ilasaca, M., Zhang, L., Solomon, S.D., Deb, A., Dzau, V.J., and Pratt, R.E. (2006). Mesenchymal stem cells overexpressing Akt dramatically repair infarcted myocardium and improve cardiac function despite infrequent cellular fusion or differentiation. Mol. Ther. *14*, 840–850.

Peng, L., Jia, Z., Yin, X., Zhang, X., Liu, Y., Chen, P., Ma, K., and Zhou, C. (2008). Comparative analysis of mesenchymal stem cells from bone marrow, cartilage, and adipose tissue. Stem Cells Dev. *17*, 761–773.

Pittenger, M.F., Mackay, A.M., Beck, S.C., Jaiswal, R.K., Douglas, R., Mosca, J.D., Moorman, M.A., Simonetti, D.W., Craig, S., and Marshak, D.R. (1999). Multilineage potential of adult human mesenchymal stem cells. Science *284*, 143–147.

Quevedo, H.C., Hatzistergos, K.E., Oskouei, B.N., Feigenbaum, G.S., Rodriguez, J.E., Valdes, D., Pattany, P.M., Zambrano, J.P., Hu, Q., McNiece, I., et al. (2009). Allogeneic mesenchymal stem cells restore cardiac function in chronic ischemic cardiomyopathy via trilineage differentiating capacity. Proc. Natl. Acad. Sci. USA *106*, 14022–14027.

Ranganath, S.H., Levy, O., Inamdar, M.S., and Karp, J.M. (2012). Harnessing the mesenchymal stem cell secretome for the treatment of cardiovascular disease. Cell Stem Cell *10*, 244–258.

Seeger, F.H., Tonn, T., Krzossok, N., Zeiher, A.M., and Dimmeler, S. (2007). Cell isolation procedures matter: a comparison of different isolation protocols of bone marrow mononuclear cells used for cell therapy in patients with acute myocardial infarction. Eur. Heart J. *28*, 766–772.

Soleimani, M., and Nadri, S. (2009). A protocol for isolation and culture of mesenchymal stem cells from mouse bone marrow. Nat. Protoc. *4*, 102–106.

Sung, J.H., Yang, H.M., Park, J.B., Choi, G.S., Joh, J.W., Kwon, C.H., Chun, J.M., Lee, S.K., and Kim, S.J. (2008). Isolation and characterization of mouse mesenchymal stem cells. Transplant. Proc. *40*, 2649–2654.

Tateishi-Yuyama, E., Matsubara, H., Murohara, T., Ikeda, U., Shintani, S., Masaki, H., Amano, K., Kishimoto, Y., Yoshimoto, K., Akashi, H., et al.; Therapeutic Angiogenesis using Cell Transplantation (TACT) Study Investigators (2002). Therapeutic angiogenesis for patients with limb ischaemia by autologous transplantation of bone-marrow cells: a pilot study and a randomised controlled trial. Lancet *360*, 427–435.

Tendera, M., Aboyans, V., Bartelink, M.L., Baumgartner, I., Clément, D., Collet, J.P., Cremonesi, A., De Carlo, M., Erbel, R., Fowkes, F.G., et al.; European Stroke Organisation; ESC Committee for Practice Guidelines (2011). ESC guidelines on the diagnosis and treatment of peripheral artery diseases: document covering atherosclerotic disease of extracranial carotid and vertebral, mesenteric, renal, upper and lower extremity arteries: the task force on the diagnosis and treatment of peripheral artery diseases of the European Society of Cardiology (ESC). Eur. Heart J. *32*, 2851–2906.

van der Bogt, K.E., Schrepfer, S., Yu, J., Sheikh, A.Y., Hoyt, G., Govaert, J.A., Velotta, J.B., Contag, C.H., Robbins, R.C., and Wu, J.C. (2009). Comparison of transplantation of adipose tissue- and bone marrow-derived mesenchymal stem cells in the infarcted heart. Transplantation *87*, 642–652.

Yamamoto, N., Akamatsu, H., Hasegawa, S., Yamada, T., Nakata, S., Ohkuma, M., Miyachi, E., Marunouchi, T., and Matsunaga, K. (2007). Isolation of multipotent stem cells from mouse adipose tissue. J. Dermatol. Sci. *48*, 43–52.

Zacchigna, S., Pattarini, L., Zentilin, L., Moimas, S., Carrer, A., Sinigaglia, M., Arsic, N., Tafuro, S., Sinagra, G., and Giacca, M. (2008). Bone marrow cells recruited through the neuropilin-1 receptor promote arterial formation at the sites of adult neoangiogenesis in mice. J. Clin. Invest. *118*, 2062–2075.

Stem Cell Reports, Volume *4*

Supplemental Information

In Vivo Therapeutic Potential of Mesenchymal Stromal Cells Depends on the Source and the Isolation Procedure

Francesca Bortolotti, Laura Ukovich, Vahid Razban, Valentina Martinelli, Giulia Ruozi, Barbara Pelos, Franca Dore, Mauro Giacca, and Serena Zacchigna

SUPPLEMENTAL FIGURES AND LEGENDS

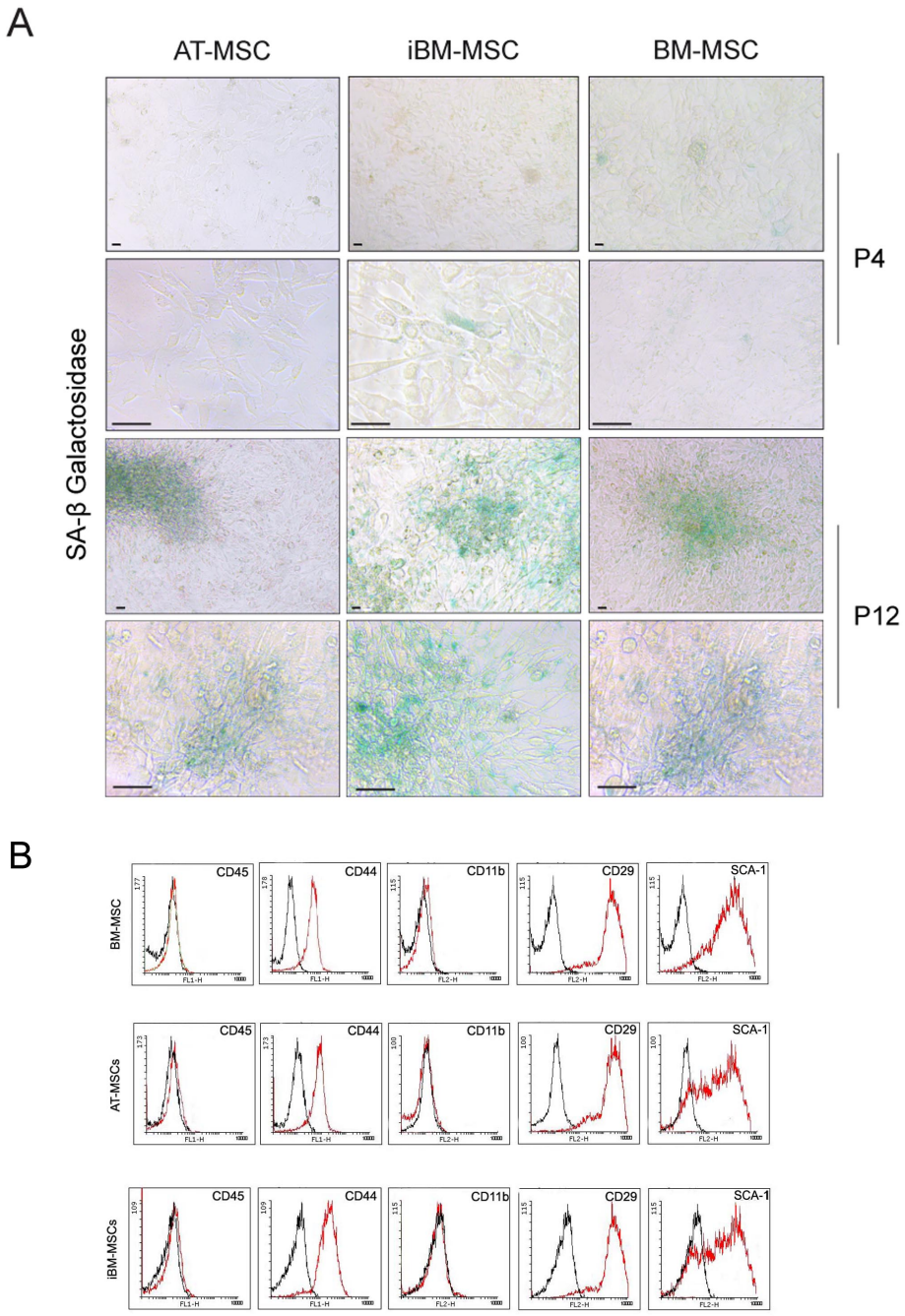

Figure S1

<u>Figure S1.</u> Characterization of cellular senescence and surface marker expression for the three MSC populations.

Related to Figure 1.

A. Representative images of senescence-associated β-galactosidase (SA-βgal) expression detected in MSC cultures, at early (4) and late (12) passages. Scale bar 50 μm for lower magnification and 10 μm for higher magnification.

B. Flow cytometry plots for the surface antigens commonly recognized as MSC markers. The black line refers to isotype control antibody, whereas the red line corresponds to the three MSC populations stained using the indicated antibodies.

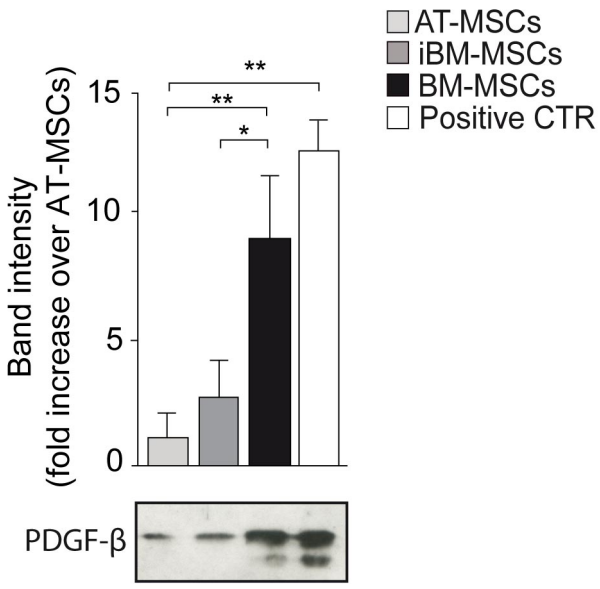

Figure S2

<u>Figure S2</u>. BM-MSCs secrete high levels of PDGF-β.

Related to figure 3.

Analysis of PDGF-β secretion by MSCs. The same number of AT-, iBM- and BM-MSCs was plated and kept in culture for 24 hours in serum-free medium. The presence of PDGF-β was detected by Western Blotting. Supernatant from PDGF-β-transfected cells was used as a positive control. Data (n=3 biological replicates) were normalized over AT-MSCs and shown as mean ± SEM (**P*< 0,05; ***P*<0,01).

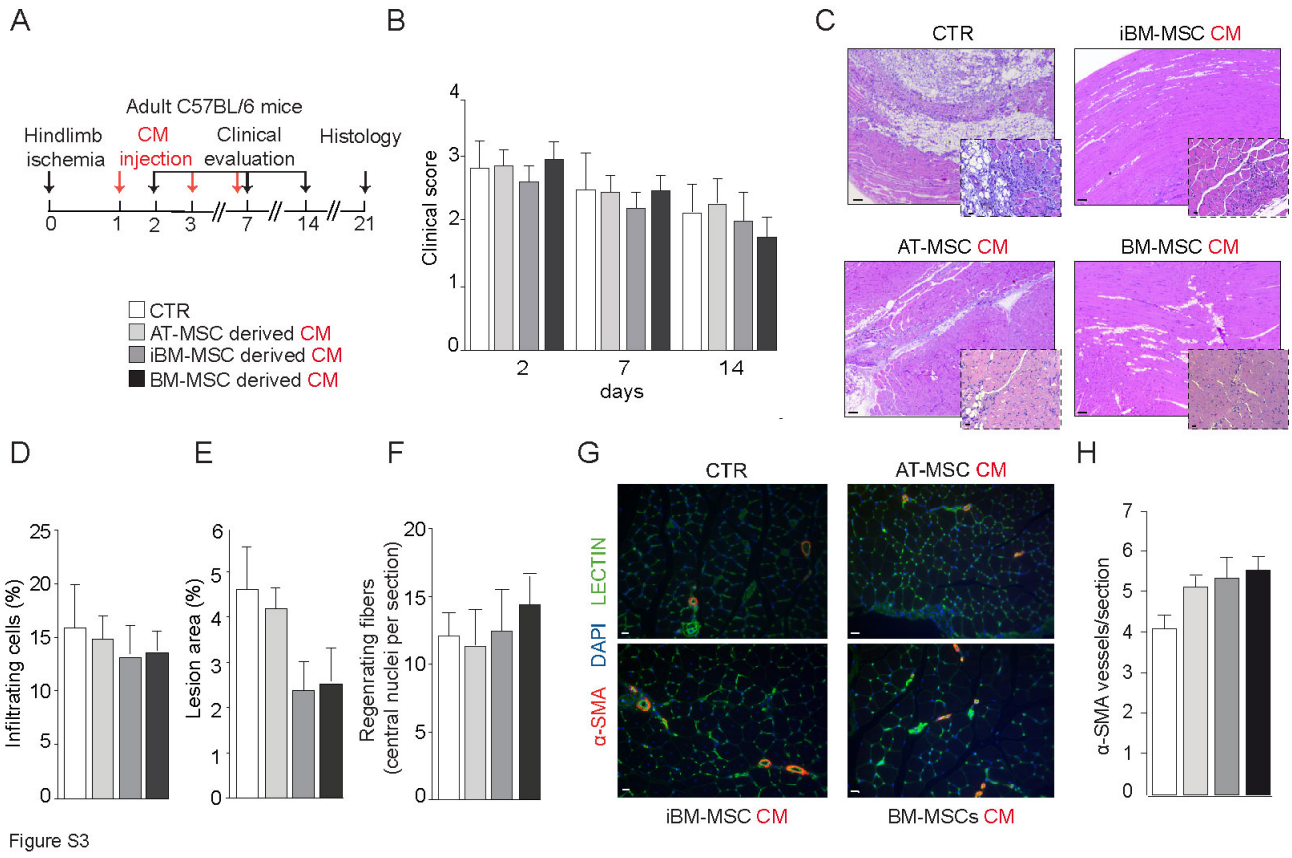

Figure S3. MSC-derived Conditioned Medium (CM) partially recapitulates the therapeutic effect of MSC administration after ischemia.

Related to Figure 3.

A. CLI experimental flow chart. Mice received concentrated CM derived from AT-, BM- or iBM- MSCs at passage 4 or medium without serum (n=6 animals for each group) at days 1, 3 and 7 after resection of the femoral artery.

B. Limb function evaluation at days 2, 7 and 21 after CLI according to the criteria described in **Table S2**.

C. Representative hematoxylin-eosin staining of ischemic muscles of untreated and treated animals at day 21. Scale bar 100 μm for lower magnification and 10 μm for higher magnification.

D. Percentage of infiltrating cells at the site of ischemia. Data are shown as mean ± SEM.

E. Percentage of muscle affected by ischemic damage. Data are shown as mean ±

SEM.

F. Quantification of central nuclei as a hallmark of muscle regeneration. Data are shown as mean ± SEM.

G. Representative immunostaining for vascular structures in ischemic muscles treated with either serum-free medium or CM derived from, AT-, BM- or iBM-MSCs at day 21. α-SMA red; LECTIN, green; DAPI, blue; scale bar 50 μm.

H. Quantification of the number of α-SMA positive vessels. The graph shows mean ± SEM.

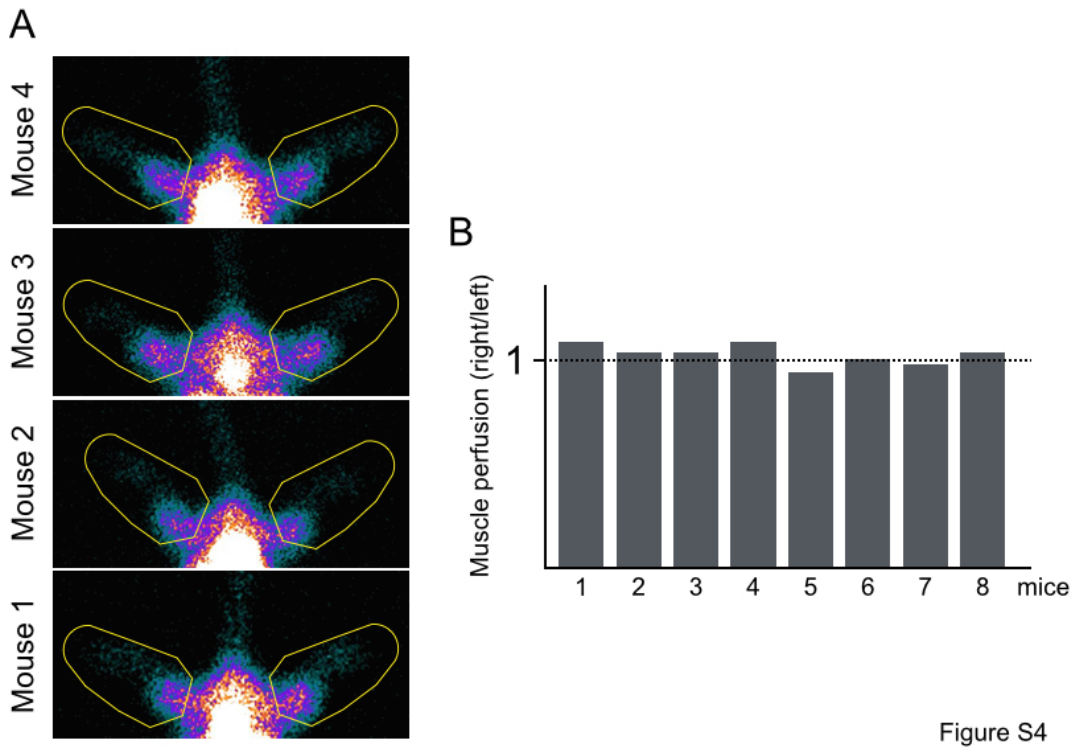

Figure S4. Planar Scintigraphy at baseline reveals equal perfusion of the two hind limbs

Related to Figure 4.

A. Representative images of planar scintigraphy showing the ROI (yellow line), used to quantify muscle perfusion on both hind limbs in 4 animals before surgery.

B. Quantification of muscle perfusion, expressed as the right to left ratio of counts within the ROI in 8 randomly selected animals before surgery.

SUPPLEMENTAL TABLES

Table S1. Surface antigen expression by cultured MSCs from different sources analyzed by flow cytometry.

Related to Figure 1.

For clarity, a symbol related to the percentage of positive cells was assigned to each marker: - < 10%; + 10-30%; ++ > 30%.

Surface antigen	AT-MSCs	BM-iMSCs	BM-MSCs
CD105	+	+	+
CD11b	-	-	-
CD29	++	++	++
CD31	-	-	-
CD34	-	-	-
CD44	++	++	++
CD45	-	-	-
CD90	+	-	+
C-KIT	+	+	+
CXCR4	+	+	+
FLK1	-	-	-
GR-1	-	-	-
SCA-1	++	++	++
TER119	+	+	+
TIE-2	+	+	+

Table S2. Score assignment criteria for evaluation of ischemic damage.
Related to Figure 2.

Score	Clinical evaluation of left hind limb
0	No differences from contralateral hind limb
1	Mild hypomobility and discoloration
2	Moderate hypomobility and discoloration
3	Severe hypomobility and distal necrosis
4	Paw dragging and massive gangrene

Table S3. List of genes analyzed for expression by real-time, quantitative PCR.

Related to Figure 3.

Gene acronym	Gene name	Ref. Seq	Real time PCR assay
Ang-1	angiopoietin 1	NM_009640.3	Mm00456503_m1
Ang-2	angiopoietin 2	NM_007426.3	Mm00545822_m1
Ccl2	chemokine (C-C motif) ligand 2	NM_011333.3	Mm00441242_m1
Ccl5	chemokine (C-C motif) ligand 5	NM_013653.3	Mm01302427_m1
Cxcr4	chemokine (C-X-C motif) receptor 4	NM_009911.3	Mm01292123_m1
Cxcl9	chemokine (C-C motif) ligand 4	NM_013652.2	Mm00443111_m1
Cxcl10	chemokine (C-X-C motif) ligand 10	NM_021274.1	Mm00445235_m1
Flt-1	FMS-like tyrosine kinase 1	NM_010228.3	Mm00438980_m1
Flk-1	kinase insert domain protein receptor	NM_010612.2	Mm00440099_m1
Mmp9	matrix metallopeptidase 9	NM_013599.2	Mm00442991_m1
Nrp-1	neuropilin 1	NM_008737.2	Mm00435372_m1
Pdgf-β	platelet derived growth factor, B polypeptide	NM_011057.3	Mm00440678_m1
Plx1	plexin A1	NM_008881.2	Mm00501110_m1
Rgs-5	regulator of G-protein signaling 5	NM_009063.3	Mm00501393_m1
Sdf-1	stromal cell-derived factor 1	NM_013655.3	Mm00445552_m1
Tgf-β	transforming growth factor, beta	NM_011577.1	Mm00441724_m1
uPa	plasminogen activator, urokinase	NM_008873.2	Mm01274460_g1
Vegf-a	vascular endothelial growth factor A	NM_009505.4	Mm00437304_m1
Gapdh	glyceraldehyde-3-phosphate dehydrogenase	NM_008084.2	Mm99999915_g1

All the amplifications were performed using pre-developed assays (Applied Biosystems).

The housekeeping gene *Gapdh* was used to normalize the results.

SUPPLEMENTAL EXPERIMENTAL PROCEDURES

Murine mesenchymal stromal cells isolation and culture

Bone marrow

Briefly, by flushing the tibia and femur bone cavity with Dulbecco's modified Eagle's medium-high glucose (DMEM-HG) supplemented with penicillin/streptomycin (P/S, 100 U/mL and 100 g/mL), a cell suspension was obtained and filtered through a 70 μm filter mesh to remove any bone spicule or muscle and cell clump. MSCs were then isolated according to two different protocols.

BM-MSCs were isolated using an adapted protocol, previously published (Soleimani and Nadri, 2009). This protocol is based on MSC physical propensity to adhere to plastic substrates and on frequent medium changes to avoid contamination by hematopoietic cells. BM-MSCs were cultured in complete medium (DMEM-HG supplemented with 10% heat-inactivated fetal bovine serum (FBS) and P/S) and non-adherent cells were removed after 3 hours, followed by fresh complete medium replacement. This step was repeated every 12 hours for 3 days. Cells reached 90% confluence in approximately 2 weeks and were lifted by incubation in 0.5 ml of 0.25% trypsin/1 mM EDTA for 2 minutes at room temperature. Lifted cells were cultured in 25-cm^2 flask until confluence at 37°C in a 5% CO_2 humidified incubator, changing the medium every 3–4 days.

iBM-MSCs isolation was based on a density gradient, followed by immunodepletion of monocytes and granulocytes (Sung et al., 2008). After bone flushing, cells were suspended in equal amount of DMEM and Hank's Balance Salt Solution (HBSS) and all mononuclear cells (MNCs) were isolated by density-gradient centrifugation using Histopaque-1077 (Sigma Chemical Co.), according to the manufacturer protocol. MNCs were then immunodepleted of monocytes and granulocytes using anti-CD11b-coupled micromagnetic beads (Miltenyi Biotec.). The residual cells were cultured in complete medium, as described above. After removal of non-adherent cells after 72–96 hours,

adherent cells were harvested by trypsinization (0.05% trypsin-EDTA) when reaching 90% confluence, and then replated. The medium was changed every 3–4 days.

Adipose Tissue

Subcutaneous adipose tissue was cut into fine pieces and digested with 1 mg/mL collagenase IA (Sigma) for 90 minutes at 37°C while shaking. The released cells were centrifuged for 15 minutes at 400g, washed with PBS twice and filtered through a 70 µm mesh. To separate MSCs from adipocytes, the cell suspension was subjected to two additional centrifugation steps at 800g. Pelleted MSCs were resuspended in lysis buffer (BD) to lyse and remove red blood cells. The residual cells were eventually cultured as described for BM-derived cells.

At least 3 independent isolations were performed for each isolation protocol.

Animal care and hind-limb ischemia

Animal care and treatment were conducted in conformity with institutional guidelines, in compliance with national and international laws and policies (European Economic Community Council Directive 86/609, OJL 358, December 12th, 1987 and UE2010763) after institutional review board approval. Mice (6-week-old female C57/BL6) were anesthetized using xylazine (40 mg/kg) and ketamine (100 mg/kg), prior to ligation and removal of the entire left femoral artery. The following day, mice were randomly divided into 4 groups (n>10) and injected intramuscularly with AT-, BM-, iBM-MSCs or medium as control. Each animal received $5x10^4$ (passage 3-5) cells in its left tibialis anterior muscle and $1,5x10^5$ cells in its left gastrocnemious muscle (final volume: 50 µl and 150 µl, respectively). Mice were repeatedly monitored for limb function, according to the parameters described in **Table S2**. At the end of the experiments (day 21), the injected muscles were harvested, embedded in paraffin and processed for histological analysis. The tibialis muscles were analyzed on transversal sections, while the gastrocnemious

muscles on longitudinal sections.

For cell fate and retention experiments, MSCs were labeled with DiI dye (Invitrogen) and administered as previously described into the left tibialis anterior and gastrocnemious muscles the day after CLI (n= 6 per group).

Planar Scintigraphy

Planar Scintigraphy was performed prior to surgery (baseline, shown for 8 representative animals in **Figure S4**), on day 1 (immediately before MSC injection), as well as on days 7 and 14 (n=8 per group). Functional images of the mouse hind limbs were acquired after the injection of 37 MBq (1 µL) of 99mTc tetrofosmin (Myoview®, GE Healthcare) into the jugular vein (small pinhole collimator hole: 4 mm; frame-acquisition time 10 min; zoom acquisition 3.2). Quantitative analysis was made by manually drawing an oval region of interest (ROI) first on the ischemic hind limb and then symmetrically applying the same ROI to the contralateral limb. ROI was demarcated paying attention to avoid abdominal radioactivity and to include limb extremities. Perfusion data at each time point were expressed as a right/left ratio to overcome inter-animal variability and eventually normalized to the perfusion measured at day1 to overcome possible differences due to the severity of muscle ischemia.

Flow cytometry

Cells surface antigens were analyzed by flow cytometry using a BD FACSCalibur. MSCs ($1x10^5$ cells at passage 3) were incubated on ice for 30 minutes in PBS, 2% BSA and stained with fluorescein isothiocyanate- (FITC-) or phycoerythrin (PE-) conjugated monoclonal antibodies against mouse CD44, CD45, CD31, CD29, CD11b, CD105, CD34, CD90, CD117 (C-KIT), TER-119, stem cell antigen (SCA)-1, CXCR4, GR-1, FLK1, TIE2 (all from BD), or isotype-matched mouse monoclonal antibodies (BD) as controls. Data are

summarized in **Table S1 and Figure S1B**.

Colony Forming Unit assay (CFU) and cell proliferation assay

For the proliferation assay murine AT-, iBM-, BM-MSCs ($1x10^5$ cells at passage 2) were plated in 6-multiwell plates and counted daily for four days. For CFU assay, MSCs (250 cells at passage 2) were plated in a 6-multiwell plate; after 10 days of culture, cells were stained with Crystal Violet and the number of colonies was counted manually. The experiments were performed in triplicate and results expressed as mean±SEM.

Differentiation assays

Differentiation was performed on cells at passage 3 using Adipolife, OsteoLife and ChondroLife complete medium, respectively (all from LifeLine Cell Technologies). Oil Red, Alizarin Red, and Alcian Blue (LifeLine Cell Technologies) staining for adipocytes, osteocytes, and chondrocytes, were performed according to the manufacturer protocols.

Histology and immunofluorescence

Cultured MSCs were immunostained for CD44 (Abcam, 1:100) and CD105 (R&D system, 1:100), followed by goat anti-rabbit or donkey anti-goat AlexaFluor 594 (Molecular Probes, 1:1000). All images were acquired using a fluorescence microscope (Leica Microsystems), equipped with a charge-coupled device camera. In all experiments, exposure and picture processing were applied equally to sample sections and controls (isotype or primary antibody present).

Muscle sections were stained with hematoxylin-eosin to perform morphometric analysis of tissue damage, cell infiltration (on longitudinal section), and fiber regeneration (on transversal section) by acquiring at least 10 images per mouse and using NIH ImageJ software for data quantification (data are expressed as mean±SEM).

To analyze tissue vascularization, sections were stained with Cy3-conjugated mouse monoclonal antibody anti-α-SMA (Sigma, 1:200), FITC-conjugated LECTIN from Triticum vulgaris (Sigma, 1:200) for 2 hours. At least 10 images per muscle were acquired and the number of arteries was expressed as the number of α-SMA-positive vessels (mean±SEM). To track cell engraftment *in vivo,* MSCs were labeled with DiI (Invitrogen) prior to injection. Injected muscles were snap frozen and cryosections were stained for 2 hours at RT with FITC-LECTIN. Quantification of retained cells was performed using the ImageJ software (9 slices every 50 μm per muscle, 6 fields per section). To track cell differentiation in vivo, muscles at 21 days were stained with rat polyclonal anti-CD31 (1:100, BD Pharmingen) or Cy3-conjugated α-SMA (1:200, Sigma) antibodies, followed by goat anti-mouse AlexaFluor 488 (1:500, Molecular Probe) or goat anti-rat AlexaFluor 488 antibody (1:500, Invitrogen), respectively.

Real-Time PCR

Total RNA was extracted from MSCs isolated according to the three experimental procedures (n=3 each) using TRIzol reagent (Invitrogen) according to manufacturer instructions, treated with DNase I (Roche) and reverse transcribed using hexameric random primers. The cDNA was then used as a template for real-time PCR amplification to detect the expression levels of the murine genes listed in **Table S3.** The housekeeping gene *Gapdh* was used to normalize the results. All the amplifications were performed on a Bio-Rad Real-time thermal cycler CFX96 using TaqMan probes (Applied Biosystem).

Migration assay

Migration assays were performed using 8 μm pore Transwell permeable supports (Costar, Corning Incorporated). MSCs (isolated from at least 3 animals per MSC type, 10^5 cells per animal) were seeded in the lower chamber, whereas mouse primary aortic smooth muscle

cells (C57-6080; CellBiologics; 1×10^4 cells) were seeded in serum-free medium in the upper chamber. After 12 hours, the upper side of the filters was carefully washed with PBS, and migrated cells on the lower surface of the membrane were fixed in PFA and stained with DAPI (Vector Lab.). Relative areas occupied by migrated cells were quantified using Image J (National Institutes of Health). Experiments were performed in triplicate by quantifying the number of migrated cells on membrane images acquired by ImageXpress Micro automated high-content screening fluorescence microscope. Data are presented as mean±SEM.

Apoptosis assay

MSC apoptosis was induced in 6-multiwell plates adding 500 μM of hydrogen peroxide (H_2O_2). The Annexin V-FITC Apoptosis Detection Kit (Roche) was used to quantify the number of apoptotic cells by flow cytometry, according to manufacturer instructions. Apoptosis induced by doxorubicin (2 μM for 12 hours) was evaluated using Caspase-Glo 3/7 Assay Systems (Promega) in 96-multiwell plates, according to manufacturer instructions and analyzed by the EnVision multilabel reader (Perkin Elmer). All experiments were performed in triplicate and data, normalized over untreated cells, are presented as mean±SEM.

Senescence assay

Senescence associated-β galactosidase (SA- β gal) was evaluated on cells at passages 4 and 12, kept in culture for 5 days. Cells were washed with PBS, fixed for 10 minutes in 4% PFA, washed in PBS and incubated at 37°C with senescence X gal stain solution (1 mg X-galactose; 40 mM citric acid/sodium phosphate at pH 6; 5mM potassium ferricyanide; 150mM NaCl; 2mM $MgCl_2$). Images of stained cells were acquired after 12 hours.

Conditioned medium preparation

MSCs ($1x10^6$ cells at passage 4) were plated in 6 cm^2 dishes and incubated in complete medium for 1 day. Cells were then washed with PBS and the medium was replaced with 1 ml of serum free medium. Media were collected after 24 hours, concentrated using the Amicon Ultra 0,5 Centrifugal Devices (cut-off 3 kDa; Millipore) and filtered through a 20 µm filter. The concentrated conditioned media (CM) were frozen and stored at -80°C. Three doses of CM corresponding to $2x10^5$ MSCs were injected in the tibialis anterior and in the gastrocnemius muscles of C57/BL6 mice at day 1, 3, 7 after surgery (n=6 animals per group). Animals were followed for 21 days for functional and histological evaluation.

Western Blot

To quantify the levels of PDGF-β secreted by the three MSC populations, CM was collected from the same number of AT-, iBM- and BM-MSCs. Samples were resolved by 10% SDS-PAGE and transferred to PVDF membranes (GE Healthcare). Immunoblots were blocked in 5% bovine serum albumin in TBS-Tween (50 mM Tris-HCl, pH 7.4; 200 mM NaCl; and 0.1% Tween 20), incubated O/N at 4^oC with primary rabbit polyclonal anti–PDGF-β antibody (sc-7878 Santa Cruz) and then with anti-rabbit HPR-conjugated secondary antibodies for 1 hour at room temperature. Proteins were detected by enhanced chemiluminescence (GE Healthcare). CM obtained after transfection of a *Pdgf-β* plasmid was used a positive control for the antibody. Band intensity was analyzed using the ImageJ software.

SUPPLEMENTAL BIBLIOGRAPHY

Dimri, G.P., Lee, X., Basile, G., Acosta, M., Scott, G., Roskelley, C., Medrano, E.E., Linskens, M., Rubelj, I., Pereira-Smith, O.*, et al.* (1995). A biomarker that identifies senescent human cells in culture and in aging skin in vivo. Proc Natl Acad Sci U S A *92*, 9363-9367.